2018
International Symposium on Power Electronics,
Electrical Drives, Automation and Motion

Darrieus Wind Turbine Prototype Control Study

Tobias Pereira[2], Nelson Batista[1,3], Carlos Cardeira[1,2], Paulo Oliveira[1,2], Rui Melicio[1,3]
[1]IDMEC, [2]Instituto Superior Tecnico, Universidade de Lisboa, Lisboa, Portugal
[3]ICT, Universidade de Evora, Escola de Ciencias e Tecnologia, Departamento de Fisica
ruimelicio@gmail.com

***Abstract*—This paper focuses on control of a Darrieus vertical axis wind turbine prototype. Throughout this work a control strategy is proposed and a methodology is presented in order to achieve a solid foundation for the control process. A non linear dynamic model of the Darrieus prototype equipped with a permanent magnet synchronous generator was developed. The model was linearized and some controllers are developed, namely a PID controller and a Linear Quadratic Regulator. The controllers were tested in the linear and non linear models.**

I. Introduction

Most wind power generation systems consist in Horizontal Axis Wind Turbines (HAWT). A solution to generate energy from wind closer to the consumer and to increase the wind power usage is the Vertical Axis Wind Turbine (VAWT). In comparison to HAWT, most VAWT models have the following advantages [6]: performance is independent from wind direction, thus not requiring any special mechanisms for yawing into wind; VAWT have the ability to generate energy from wind skewed flows; smaller number of components; low sound emission; blades can be manufactured by mass production extrusion, since they are often untwisted and of constant chord; ability to operate closer to the ground and, for large dimensions VAWT, the generator is usually installed on the base, which makes maintenance simpler and cheaper.

This works presents a structured method to elaborate linear and non linear models for the main subsystems and how to interpret their interaction. Furthermore, the controllers of the controlled system are derived and simulated.

II. VAWT Dynamic Modeling

A. Turbine

The available kinetic energy stored in the wind is calculated taking into account the assumption that all particles presented in the wind are moving at constant speed and direction.

The aerodynamic torque T_a is given by:

$$T_a = \rho r^2 H C_p(\lambda)\nu^2 \frac{1}{\lambda} \tag{1}$$

where, ρ is the air density, r and H are the turbine radius and middle height, C_p is the power coefficient, λ is the Tip Speed Ratio (TSR), ν the wind speed.

The TSR represents the interaction between the rotor and the wind flow. For HAWT it is defined by the quotient between the tangential linear speed of the rotor at the tip of the blade and the wind speed, that is perpendicular to the swept area of the blades. For the VAWT it is more complicated since there are two tips of the blade and depending on their design the tips can be closer or farther to the rotating axis. Since for the turbine considered the tips are closer to the rotating axis than the middle section of the blade, the TSR will be calculated at middle height of the turbine.

Previous studies have achieved a theoretical relation between C_p and λ. Fig.1 shows both theoretical an experimental data [2].

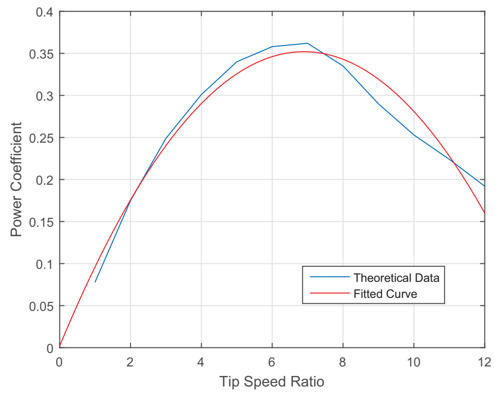

Fig. 1. C_p in function of the TSR (λ).

This experiment was performed with a uniform wind speed of 12 m/s. Using the fitted curve that describes the behavior of C_p in function of the TSR, the aerodynamic torque T_a is given by:

$$T_a = \rho r H(-0.007365\lambda^2 + 0.1015\lambda + 0.002052)\ \nu^3\ \omega^{-1} \tag{2}$$

where ω is the rotor angular speed.

Linearizing the aerodynamic torque due to the wind impact on the turbine blades, as a Taylor series yields:

$$T_a(\nu, \omega) \approx \overline{T_a} + a\ \delta\nu + b\ \delta\omega \tag{3}$$

where $\overline{T_a}$ is the nominal aerodynamic torque, $\delta\nu$ is the wind speed variation and $\delta\omega$ is the rotor angular speed variation.

Hence, $\delta\nu = \nu - \overline{\nu}$, $\delta\omega = \omega - \overline{\omega}$ and a and b are given by:

$$a = \left.\frac{\partial T_a}{\partial \nu}\right|_{opt} \ and\ b = \left.\frac{\partial T_a}{\partial \omega}\right|_{opt} \tag{4}$$

978-1-5386-4941-1/18/$31.00 ©2018 IEEE

B. Generator

The electrical model of the Permanent Magnet Synchronous Generator (PMSG) in the synchronous reference frame was presented in [8]- [9]. Considering the simplification regarding inductances ($L_d = L_q$), the electromagnetic torque is given by:

$$T_{em} = 1.5 n_p \lambda_o i_q \tag{5}$$

Some tests performed on the PMSG with an auxiliary motor were developed in order to obtain a relation between the generator behavior regarding the angular speed of the rotor. Two of those tests were performed with the generator in open and short circuit.

The PMSG functions for open circuit voltage and short circuit current are given by:

$$U(\omega) = 0.2841\ \omega + 0.2193\ (V) \tag{6}$$

$$I(\omega) = 0.0089\ \omega - 0.0004\ (A) \tag{7}$$

For all situations, applying a referential transform to the variables in study in module, corresponds to a positive gain. Therefore we have that:

$$u_q = 1.5\ \sqrt{\frac{2}{3}}\ U\ and\ i_q = 1.5\ \sqrt{\frac{2}{3}}\ I \tag{8}$$

For the following steps $i_{q_{ref}} = 0$ and $u_{q_{ref}} = 0$, however regarding the dynamics of the generator, for transient situations this will not be true due to (10).

Using (6) and (7), the state space representation variables can be replaced by direct relations to the angular speed of the turbine. The modified state space is given by:

$$\begin{aligned} \frac{di_q}{dt} = -\frac{R}{L}\ 1.5\ \sqrt{\frac{2}{3}}\ (0.0089\ \omega - 0.0004) - n_p\ \omega\ \frac{\lambda_o}{L} \\ - n_p\ \omega\ i_d + \frac{1}{L}\ 1.5\ \sqrt{\frac{2}{3}}\ (0.2841\ \omega + 0.2193) \end{aligned} \tag{9}$$

$$\frac{di_d}{dt} = n_p\ \omega\ i_q \tag{10}$$

In order to apply a control strategy that uses as actuation a variable circuit resistance, it is required to achieve the relation between this actuation R_c in the *abc* (physical) referential to the corresponding to a *dq0* referential, in order to relate circuit resistance R_c to the current i_q. Knowing that, for a closed circuit with resistive loads R is given by:

$$R = R_a + R_c \tag{11}$$

where R_a is the sum of the PMSG coil resistances, R_c is the circuit imposed load resistance in the *dq0* referential, that will be the variable to control. Linearizing (9) and (10) around a generic operating point, the linearized equations are given by:

$$\delta \dot{i}_q \approx c\ \delta R_c + d\ \delta\omega + g\ \delta i_d \tag{12}$$

$$\delta \dot{i}_d \approx j\ \delta\omega + k\ \delta i_q \tag{13}$$

where $\delta \dot{i}_q = \dot{i}_q - \overline{\dot{i}_q}$, $\delta \dot{i}_d = \dot{i}_d - \overline{\dot{i}_d}$, $\delta R_c = R_c - \overline{R_c}$ and c, d, g,j and k are given by:

$$c = \left.\frac{\partial \dot{i}_q}{\partial R_c}\right|_{opt}\ and\ d = \left.\frac{\partial \dot{i}_q}{\partial \omega}\right|_{opt} \tag{14}$$

$$g = \left.\frac{\partial \dot{i}_q}{\partial i_d}\right|_{opt}\ and\ j = \left.\frac{\partial \dot{i}_d}{\partial \omega}\right|_{opt} \tag{15}$$

$$k = \left.\frac{\partial \dot{i}_d}{\partial i_q}\right|_{opt}\ and\ e = \left.\frac{\partial T_{em}}{\partial i_q}\right|_{opt} \tag{16}$$

Linearizing around an operating point (opt), the electromagnetic torque expressed in equation (5) is given by:

$$T_{em} \approx \overline{T_{em}}\ + e\ \delta i_q \tag{17}$$

where $\delta i_q = i_q - \overline{i_q}$.

C. Drive-Train

To calculate the applied aerodynamic torque, it is required to make several assumptions to account for the motion of the drive-train. The rotor is assumed to act as a rigid body and therefore, to have the same acceleration over the entire axis of rotation. Aerodynamic effects are integrated over the length of the blade and added up for all the blades.

Applying the rotational version of Newtons second law, adding moments about the vertical axis, a general equation is given by:

$$J_t \ddot{\theta} = J_t \dot{\omega} = T_a - T_{em} - \beta\omega \tag{18}$$

where, J_t is the total inertial moment of the VAWT, T_a is the aerodynamic torque, T_{em} is the measured torque on the generator and β is the damping coefficient.

For the configuration in hand, the axle has a small distance between supports and for the vertical position it is valid to look down on vibrations of mechanical deformation of the axis due to flexion and torsion originated by non uniform speed and direction in wind flow.

For a better understanding of the system in order to lastly apply a control strategy it is important to have a main equation, which appears by merging (18) with the linearized quantities of interest.

Using (3) and (17) in (18), and applying Laplace transform to the linear relation between the variables of interest, (19) is obtained.

$$\begin{aligned} s\ \Delta\omega(s) \approx \frac{1}{J_t}\Big(\overline{T_a} + a\ \Delta\nu(s) + b\ \Delta\omega(s) - \overline{T_{em}} - \\ e\ \Delta i_q(s) - \beta\Delta\omega(s) - \beta\overline{\omega}\Big) \end{aligned} \tag{19}$$

where a, b and e are given by:

$$a = \left.\frac{\partial T_a}{\partial \nu}\right|_{opt}\ and\ b = \left.\frac{\partial T_a}{\partial \omega}\right|_{opt} \tag{20}$$

$$e = \left.\frac{\partial T_{em}}{\partial i_q}\right|_{opt} = 1.5\ n_p\ \lambda_o \tag{21}$$

Considering $\overline{T_{em}} = \overline{T_a} - \beta\ \overline{\omega}$ and $\beta = 0$ the following simplification is obtained:

$$\delta\dot{\omega} \approx \frac{1}{J_t}\left(a\ \delta\nu + b\ \delta\omega - e\ \delta i_q\right) \tag{22}$$

In this work, studies regarding the damping coefficient are not performed, the damping coefficient represents the linearized aerodynamic damping effects plus the mechanical damping present in the drive train and in the PMSG.

III. Control Analysis

The main objectives of the control strategy implementation will be the achievement of the nominal power generated. When the nominal power is achieved the objective shifts to a new goal that is maintaining the generated power. For instance, when at nominal power generated, assuming wind speed increase, it is required to reduce C_p in order to negatively affect the turbines efficiency and therefore cancel the corresponding increment in power. Hence, from (18) it is possible to create a schematic model that describes the interaction between the different subsystems that compose the wind turbine. The closed loop model with the controller is shown in Fig. 2 where it is direct that the control variable used is δR_c.

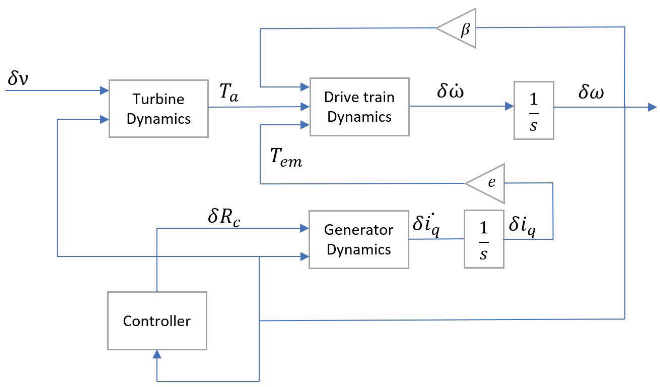

Fig. 2. Linear model scheme with controller.

A. Frequency Analysis

1) Second-Order Model: A simplified set of equations describing the TF between both inputs and the output is given by:

$$TF1^2 = \frac{\Delta\omega(s)}{\Delta\nu(s)} = \frac{a\ s}{J_t\ s^2 - b\ s + e\ d} \tag{23}$$

$$TF2^2 = \frac{\Delta\omega(s)}{\Delta R_c(s)} = \frac{-e\ c}{J_t\ s^2 - b\ s + e\ d} \tag{24}$$

The control strategy analysis and simulations are derived from (23) and (24). The output power is given by:

$$P_{out} = 1.5 n_p \lambda_o i_q \omega - R{i_q}^2 \tag{25}$$

Where R is given by (11). Linearizing (25), the output power is given by:

$$P_{out} \approx 1.5 n_p \lambda_o \overline{i_q} \Delta\omega + (1.5\lambda_o\overline{\omega} - 2R\overline{i_q})\Delta i_q + \overline{P_{out}} \tag{26}$$

To study the stability a *Root Locus* analysis is performed. To characterize the frequency response a *Bode* analysis is presented.

For the second order model assuming that the damping coefficient is negletable ($\beta \approx 0$), $TF2^2$ (24) is given by:

$$TF2^2 = \frac{\Delta\ \omega(s)}{\Delta R_c(s)} = \frac{868.9}{s^2\ + 1.1507 \times 10^{-3} s - 0.4} \tag{27}$$

By the *Root Locus* analysis it is clear that the system is marginally stable, that is, for $K = 0$ it is unstable, however for $K > 0.00046$ the system becomes stable. Therefore it is required to use a controller that has a gain higher than 0.00046.

IV. State Space Analysis

The state variables chosen are $\delta\omega$ and δi_q, since they represent the energy of the system in study. Using the state vector $\mathbf{x} = \begin{bmatrix}\delta\omega & \delta i_q\end{bmatrix}^T$ and the ouput vector $\mathbf{y} = \begin{bmatrix}\delta\omega\end{bmatrix}$, it is possible to infer that the state space representative of the system is given by:

$$\begin{cases}\dot{\mathbf{x}}(t) = \mathbf{A}\mathbf{x}(t) + \mathbf{B}\ \mathbf{u}(t) + \mathbf{E}\ \delta\nu(t)\\ \dot{\mathbf{y}}(t) = \mathbf{C}\mathbf{x}(t) + \mathbf{D}\mathbf{u}(t)\end{cases} \tag{28}$$

where $\delta\nu$ is the disturbance and $\mathbf{u} = \delta R_c$.

A. Second-Order Model

For the second-order model the parameters $\mathbf{A}$, $\mathbf{B}$, $\mathbf{C}$ and $\mathbf{E}$ are given by:

$$\mathbf{A} = \begin{bmatrix} b\ J^{-1} & -e\ J^{-1} \\ d & 0 \end{bmatrix},\quad \mathbf{B} = \begin{bmatrix} 0 \\ c \end{bmatrix} \tag{29}$$

$$\mathbf{C} = \begin{bmatrix} 1 & 0 \end{bmatrix},\quad \mathbf{D} = \begin{bmatrix} 0 \end{bmatrix},\quad \mathbf{E} = \begin{bmatrix} a\ J^{-1} \\ 0 \end{bmatrix} \tag{30}$$

1) System Characterization: With the view to characterize the system in hand, it is required to analyze its controllability, observability and stability.

Controllability

The state controllability matrix is given by:

$$\mathbf{C_s} = \begin{bmatrix} 0 & a\ J^{-1} & -e\ c\ J^{-1} & b\ a\ J^{-2} \\ c & 0 & 0 & d\ a\ J^{-1} \end{bmatrix} \tag{31}$$

From this analysis, it can be stated that the system is completely state controllable (for nonzero parameters) since the vectors $\mathbf{B}, \mathbf{AB}, ..., \mathbf{A^{n-1}B}$ are linearly independent which is the same that having the controllability matrix of $rank\ = n =\ 2$.

Observability

The state observability matrix is given by:

$$\mathbf{O} = \begin{bmatrix} 1 & 0 & -b\ J^{-1} & d \\ 0 & 1 & -e\ J^{-1} & 0 \end{bmatrix} \tag{32}$$

For the observability the rank of the matrix is 2. Hence, the system is completely observable.

Stability

Regarding stability of the system, by resorting to the Lyapunov 2^{nd} method for linear systems in order for the system to be asymptotically stable it is a necessary and sufficient condition that for a given hermitian positive defined matrix $\mathbf{Q}$, exist a hermitian positive defined matrix $\mathbf{P}$ such that the following relation is proved:

$$\mathbf{A}^*\mathbf{P} + \mathbf{P}\mathbf{A} = -\mathbf{Q} \tag{33}$$

where $\mathbf{A}^*$ is the conjugate transpose of $\mathbf{A}$. Since for the imposed conditions there is no matrix $\mathbf{P}$ that for any $\mathbf{Q}$ positive defined is positive defined as well, stability cannot be proved by now. However, this will be the subject of future work.

B. PID Controller Design

The loop was closed and a *PID(s)* controller was implemented after a fine tune. For the controlled system, the desired characteristics of the time response were, M_p (maximum overshoot) ≤ 0.2 and $t_s[2\%]$ (settling time) $\leq 10s$. From (19) the following block diagram describing the controlled system developed, is shown in Figure 3.

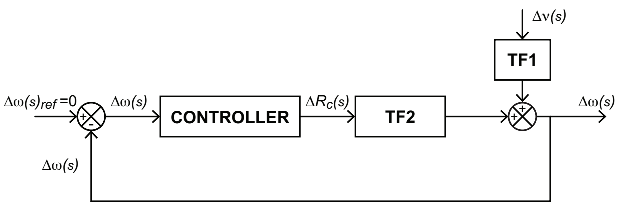

Fig. 3. Controlled system block diagram.

The controller specifications chosen are given by:

$$P = 0.0084, \quad I = 0.0033, \quad D = 0.0047, \quad N = 67.64 \tag{34}$$

The global TF of the proposed Model for the closed control loop is given by:

$$CL = \frac{TF2^2\ G(s)}{1 + TF2^2\ G(s)} \tag{35}$$

$$CL = \frac{283.51\ s\ (s+67.64)\ (s+1.163)}{s\ (s+67.64)\ (s+63.28)\ (s-0.633)\ (s+0.5986)} \cdots$$
$$\cdots \frac{(s+0.5986)\ (s+0.6319)\ (s^2+3.76s+5.119)}{(s+0.6319)\ (s^2+3.76s+5.119)} \tag{36}$$

Some mathematical models will have infinite gain/phase margins. No real-physical system has infinite margins but this will be an indication that the real-physical system has large margins. Infinite gain margin implies that a stable system is inherently stable for higher gains.

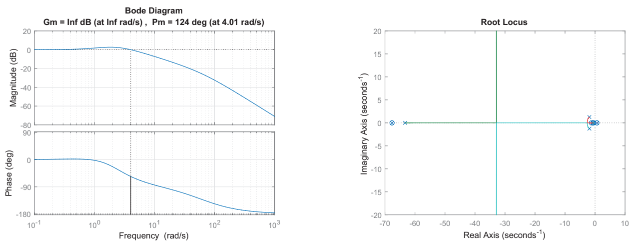

(a) Bode Analysis (b) Root Locus Analysis

Fig. 4. PID controlled system analysis: (Second-Order Model).

The *Root Locus* and *Bode* analysis is performed and shown in Figure 4.

C. LQR Controller Design in Continuous Time-Infinite Horizon

In order to design an optimal control solution the problem is solved for infinite time, being therefore a sub-optimal controller. For that achievement it is required to define some steps.

1) Control law: The control law is given by:

$$\mathbf{u} = -\mathbf{K}\ \mathbf{x} \tag{37}$$

2) Performance index: The performance index is given by:

$$J = \int_{t_0}^{t_f} [\mathbf{x}^T(t)\mathbf{Q}\mathbf{x}(t) + \mathbf{u}^T(t)\mathbf{R}\mathbf{u}(t)]dt \tag{38}$$

3) Weight matrices definition: For the state space matrices the values are tuned by performing several experiments simulating the model. Since $\mathbf{R}$ is related to the cost of energy, a higher $\mathbf{R}$ corresponds to a smaller gain, minimizing the energetic cost of the actuation. $\mathbf{Q}$ is related to how well do we want a state to follow a reference by minimizing the mean state error between the reference itself and the actual state. The weight matrices selected were tuned for each model.

4) Second-Order Model: The $\mathbf{Q}$ and $\mathbf{R}$ matrix for the second order model are given by:

$$\mathbf{Q} = \begin{bmatrix} 5 & 0 \\ 0 & 1 \end{bmatrix} \quad and \quad \mathbf{R} = [1] \tag{39}$$

5) Riccati's algebric equation - Obtaining $\mathbf{K}$*:* The Riccati's algebric equation is given by:

$$\mathbf{A}^T\mathbf{P} + \mathbf{P}\mathbf{A} - \mathbf{P}\mathbf{B}\mathbf{R}^{-1}\mathbf{B}^T + \mathbf{Q} = \mathbf{0} \tag{40}$$

where, $\mathbf{K}$ is given by:

$$\mathbf{K} = \mathbf{R}^{-1}\mathbf{B}^T\mathbf{P} \tag{41}$$

Solving the previous equations, the following gains are determined for each model.

6) Second-Order Model: The LQR controller gains for the second order model are given by:

$$\mathbf{K} = \begin{bmatrix} 2.24 & -1.54 \end{bmatrix} \tag{42}$$

V. Control solution performance

In this section the simplified model is used and simulated to have a grasp on the control strategy intended to implement. Although it is a model with reduced complexity since it does not include the dynamics associated with δi_d, the expected behavior is similar and therefore of interest. After executing the process required to obtain the LQR controller, it is possible to study the systems behavior, performing a comparison to the system controlled by the PID controller, with the tuned specifications. The Figures presented in the following subsections display behaviors of both controllers previously studied, that is, the PID and the LQR controllers. The simultaneous display intends to ease the observation of the main differences between both controllers. Wind speed is considered at its nominal value, $6\ m/s$. For all simulations, the output variable is $\delta\omega$ (angular speed variation) and the control signal is δR_c (circuit resistance variation). The wind perturbation is expressed as $\delta\nu = 4m/s$ at $t = 10s$. For the power coefficient variation analysis it is clear that the immediate wind speed increase is followed by a instant reduction of TSR resulting in a power loss and therefore a smaller power coefficient C_p. Such reduction in the TSR can only be contradicted by an increase of angular speed, which occurs by regulating the circuit resistance, which affects the passing current that affects the electromagnetic torque resulting in a change of angular speed.

The integration method used for solving the state equations of the system is Runge-Kutta of 4^{th} order of integration. This method allows integration time steps of low amplitude, allowing for high precision results. This method is simple and robust and recognized has a good generic method for integrating equations.

A. Linear Model

In this section the system is disturbed by an increase in wind speed that takes the form of a step input. It is important to notice that such disturbances are not observable in the wind behavior, it either takes the form of a ramp or of a more complex input. However for controller analysis purposes a step is valid since it represents the most abrupt way a disturbance can act on a system.

1) Second-Order Model: Since linearizing non linear equations produces linear equations for the variables perturbation, the reference for the state variable $\delta\omega$ to follow is given by:

$$\delta\omega_{ref} = \omega_{opt}(t) - \omega_{opt}(o) \tag{43}$$

The simulation results of the angular speed variation and the TSR variation with the wind speed increase are shown in Figure 5.

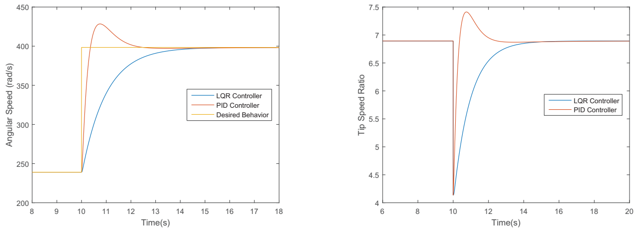

(a) Angular Speed Behavior (b) Tip speed ratio variation

Fig. 5. Angular speed behavior and TSR variation - Linear Model.

Although the LQR controller does not present overshoot, the settling time is considerably longer when compared to the PID controller, but for the problem at hand does not present any inconvenience. The simulation results of the circuit resistance variation (input) and the i_q variation with the wind speed increase are shown in Figure 6.

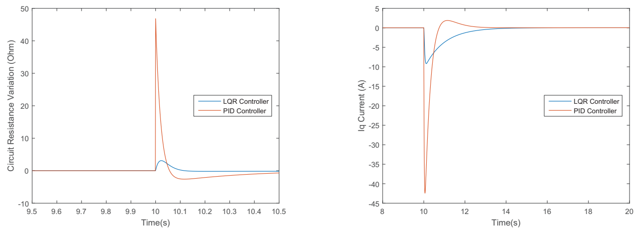

(a) Rc variance behavior (b) Iq current behavior

Fig. 6. Circuit resistance variation and Iq current behavior - Linear Model.

Although not clearly visible, after the wind speed increase at $t = 10s$ and the respective system time response, when at steady state there are slight differences in δR_c and i_q shown for the PID and LQR controller in Table I.

TABLE I
PID and LQR Controller System Parameters variation, δR_c and i_q, due to wind speed increase

Wind regime	$t < 10\ s$	$t > 10\ s$
PID		
$\delta R_c\ (\Omega)$	0	0
$i_q\ (A)$	0.0169	0.039
LQR		
$\delta R_c\ (\Omega)$	0	− 0.089
$i_q\ (A)$	0.0169	0.039

2) Same Actuation range: In order to evaluate both controllers, input variations were set to have approximately the same range of actuation to understand how well the controller is appropriate to cause the desired effect in the turbines angular speed. The respective simulation results of the angular speed variation and the circuit resistance variation with the wind speed increase are shown in Figure 7.

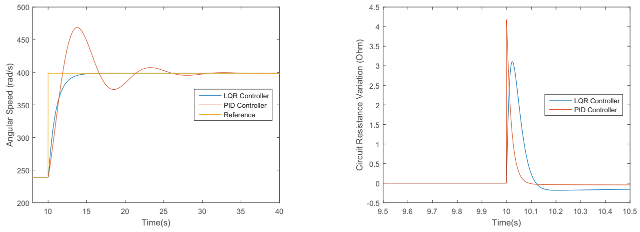

(a) Angular Speed Behavior (b) Rc Variance Behavior

Fig. 7. Angular speed and Rc variation behavior - Linear Model.

B. *Non-Linear Model*

In this section a comparison between controllers in the non linear models is shown only for the second order model. The simulation results of the non linear model for the angular speed variation and the TSR variation with the wind speed increase are shown in Figure 8.

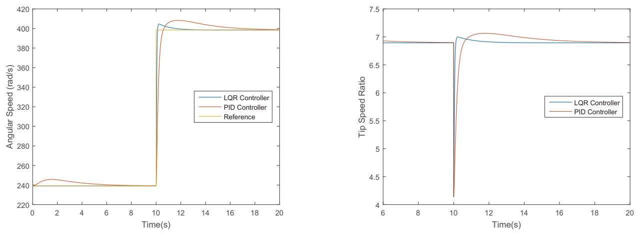

(a) Angular Speed Behavior (b) Tip speed ratio variation

Fig. 8. Angular speed behavior and TSR variation - Non Linear Model.

Here, it is clear that the LQR controller allows a better performance of the system, showing less overshoot and a smaller settling time. In the initial moments the PID controller takes a few seconds to achieve the nominal value. The specifications regarding maximum overshoot and settling time are achieved for both controllers. It's clear that the LQR controller in order to have a better response requires higher variations of input (δR_c). The simulation results of the circuit resistance variation (input) and the i_q variation with the wind speed increase are shown in Figure 9.

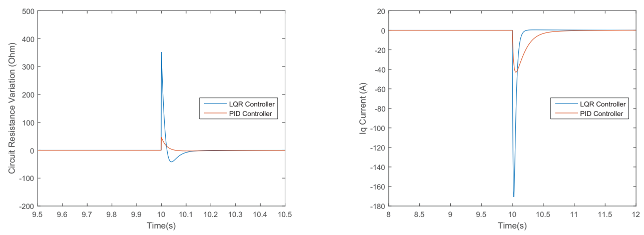

(a) Rc Variance Behavior (b) Iq Current Behavior

Fig. 9. Circuit resistance variance and Iq current behavior - Non Linear Model.

Although not clearly visible, after the wind speed increase at $t = 10s$ and the respective system time response, when at steady state there are slight differences in δR_c and i_q shown for the PID and LQR controller in Table II.

TABLE II
PID AND LQR CONTROLLER SYSTEM PARAMETERS VARIATION, δR_c AND i_q, DUE TO WIND SPEED INCREASE

Wind regime	$t < 10\ s$	$t > 10\ s$
PID		
$\delta R_c\ (\Omega)$	-0.06	-0.0892
$i_q\ (A)$	0.0169	0.0468
LQR		
$\delta R_c\ (\Omega)$	-0.06	$-\ 0.0892$
$i_q\ (A)$	0.0169	0.0468

VI. CONCLUSION

A control strategy based on the imposed circuit resistance is proposed for the linear model and simulated. Two controllers are develloped, namely a PID controller and a Linear Quadratic Regulator. The controllers were tested in the linear and non linear models.

ACKNOWLEDGMENTS

This work is funded by Portuguese Funds through the Foundation for Science and Technology FCT under the project LAETA, reference UID/EMS/50022/2013.

REFERENCES

[1] Kandpal TC, Broman L. Renewable energy education: a global status review. Renew. Sustain. EnergyRev. 2014;34:300-24.

[2] NC Batista, R Melicio, JCO Matias, JPS Catalão. New blade profile for darrieus wind turbines capable to self-start. Renewable Power Generation Conference, 1-5, Edinburgh, UK, Sep. 2011.

[3] NC Batista, R Melicio, VMF Mendes, M. Calderón, and A Ramiro. On a self-start Darrieus wind turbine: Blade design and field tests. Renewable and Sustainable Energy Reviews, 52:508-522, 2015.

[4] NC Batista, R Melicio, V Mendes, J Figueiredo, AH Reis Darrieus wind turbine performance prediction: computational modeling. Technological Innovation for the Internet of Things, SPRINGER, 394:382-391, April 2013.

[5] NC Batista, R Melicio, JCO Matias, and JPS Catalão. Self-start performance evaluation in darrieus-type vertical axis wind turbines: methodology and computational tool applied to symmetrical airfoil. International Conference on Renewable Energies and Power Quality, 1-6, Las Palmas de Gran Canaria, Spain, April 2011.

[6] NC Batista, R Melcio, JCO Matias, JPS Catalo. Self-start evaluation in lift-type vertical axis wind turbines: methodology and computational tool applied to asymmetrical airfoils. 3th International Conference on Power Engineering, Energy and Electrical Drives, pp. 1-6, Mlaga, Spain, May 2011.

[7] NC Batista, R Melicio, JCO Matias, JPS Catalão. Vertical axis wind turbine performance prediction: an approach to the double multiple streamtube model. International Conference on Renewable Energies and Power Quality, 1-4, Santiago de Compostela, Spain, March 2012.

[8] R Melicio, VMF Mendes, JPS Catalão. A pitch control malfunction analysis for wind turbines with permanent magnet synchronous generator and full-power converters: proportional integral versus fractional-order controllers. Electric Power Components and Systems, 38(4):387-406, January 2010.

[9] B. Boukhezzar, L. Lupu, H. Siguerdidjane, M. Hand. Multivariable control strategy for variable speed, variable pitch wind turbines. Renewable Energy, 32(8):1273-1287, 2007.

[10] T. Marques. Control and operation of a vertical axis wind turbine, MSc. Thesis, Lund University, June 2014.

[11] LG González, E Figueres, G Garcerá, O Carranza. Dynamic response analysis of small wind energy conversion systems (WECS) operating with torque control versus speed control. ICREPQ, 1-5, April 2009.